Artificial Organs
20(6):582–590, Blackwell Science, Inc., Boston
© 1996 International Society for Artificial Organs

Prototype Continuous Flow Ventricular Assist Device Supported on Magnetic Bearings

P.E. Allaire, *H.C. Kim, E.H. Maslen, *D.B. Olsen, and *G.B. Bearnson

*Mechanical, Aerospace, and Nuclear Engineering, University of Virginia, Charlottesville, Virginia; and *Artificial Heart Laboratory, University of Utah, Salt Lake City, Utah, U.S.A.*

Abstract: This article describes a prototype continuous flow pump (CFVAD2) fully supported in magnetic bearings. The pump performance was measured in a simulated adult human circulation system. The pump delivered 6 L/min of flow at 100 mm Hg of differential pressure head operating at 2,400 rpm in water. The pump is totally supported in 4 magnetic bearings: 2 radial and 2 thrust. Magnetic bearings offer the advantages of no required lubrication and large operating clearances. The geometry and other properties of the bearings are described. Bearing parameters such as load capacity and current gains are discussed. Bearing coil currents were measured during operation in air and water. The rotor was operated in various orientations to determine the actuator current gains. These values were then used to estimate the radial and thrust forces acting on the rotor in both air and water. Much lower levels of force were found than were expected, allowing for a very significant reduction in the size of the next prototype. Hemolysis levels were measured in the prototype pump and found not to indicate damage to the blood cells. **Key Words:** Ventricular assist device—Continuous flow pump—Magnetic bearings.

Currently, commercially available continuous flow centrifugal external blood pumps are employed routinely by heart surgeons for external use over a period of hours. For example, Joyce et al. (1) and Noon (2) describe one such external pump (the Abiomed BVS 5000) for cardiac bypass situations that has been employed routinely in postcardiotomy settings and in other cardiogenic shock cases. These devices are not suitable for long-term use but do indicate that the human body does not need pulsatility in the short term.

There are several potentially viable bearing choices for continuous flow blood pumps: ball bearings, fluid film bearings, and noncontacting magnetic bearings. Ball bearings cannot be lubricated directly with blood because extensive damage to the red blood cells is caused when the blood flows through the ball-race clearances. Ball bearings can only be used with a purged seal system. Seal failures have resulted in the failure of many continuous flow pumps. Additionally, seals accumulate protein buildup and/or thrombosis (clotting). Blood-lubricated bearings tend to be subject to high shear because of the high rotational speeds and small clearances used.

There are a number of prototype continuous axial flow ventricular assist devices (VAD), with some of the more prominent ones noted below. A catheter-mounted axial flow pump with a bearing-seal rinsing-purge pump system is used widely in Europe but is limited to intraoperative use in the United States (3,4). Macris et al. (5) discuss an example of a nonmagnetic bearing–supported electrically driven axial flow pump (the Jarvik 2000), which has evolved over many prototypes, modified to solve particular operational problems. Butler et al. (6) describe another axial flow pump (the Nimbus Axipump) on blood bearings that requires a purged seal upstream of the impeller.

Akamatsu et al. (7–9) report a pump that has a centrifugal impeller suspended magnetically. It is not fully magnetically suspended because the pump impeller is magnetically coupled to a brushless DC motor supported on rolling element bearings. O'Hara and Nosé (10) discuss a centrifugal pump (the Baylor-Gyro pump) supported on blood bear-

Received January 1996.
Address correspondence to Dr. Paul Allaire, School of Engineering and Applied Science, Department of Mechanical, Aerospace, and Nuclear Engineering, University of Virginia, Thornton Hall, Charlottesville, VA 22903-2037, U.S.A.

Abbott v. Miracor, IPR2025-00113
Abbott Ex. 1028, p. 1 of 9

ings. The most recent pump of this type has been supported on three impeller-based ball tips that ride on the housing. To date, there has not been a fully magnetically supported VAD reported in the literature.

Magnetic bearings offer the advantages of noncontact suspension, thus there is no wear over time and no friction effects (11). Additionally, large clearances can be employed between the impeller and the housing to minimize hemolysis and thrombosis. The potential for use in VAD systems was first reported by Bramm and colleagues (12). A prototype device was suspended magnetically. Olsen and Bramm (13) reported further work related to the device.

There is widespread industrial experience with low viscosity fluid film bearings in pumps having high bearing failure rates (14). Magnetic bearings are now under development as replacements for the conventional bearings to remove these failures (14,15), and they should offer the same improvement for VAD bearings (16). The large clearance allows for high circulation rates around the rotating impeller.

This article describes the development of a prototype VAD consisting of a centrifugal pump supported in a 5-axis, active, magnetic bearing system. The prototype was successfully designed, constructed, levitated on the magnetic bearings, and tested for pump performance in water and in blood. The primary emphasis of this paper is on the active magnetic bearing system rather than on pump or motor performance.

VENTRICULAR ASSIST DEVICE

The expected use of the Continuous Flow Ventricular Assist Device Number 2 (CFVAD2) system in an adult human is illustrated in Fig. 1. The pump itself will be implanted in the abdominal cavity, but the batteries and patient controller will be located external to the body in a suspender/belt system. The CFVAD2 is a blood pump that will pump blood directly to assist the left ventricle. It also could be configured to assist the right ventricle. A continuous flow VAD must be designed for long-term life, that is, more than 5 years, at a high level of reliability. It must be compatible with the anatomic space available and be hemocompatible.

The CFVAD2 has been constructed, and preliminary performance tests have been conducted on a simulated human cardiac test loop. The inlet to the CFVAD2 is a 14 mm internal diameter (ID) cannula that collects blood from the apex of the left ventricle and returns it through the outlet near the root of the aortic arch. The cardiac output will be in the range of 6–10 L/min, and the differential pressure will be approximately 100 mm Hg. The CFVAD2 will vary its cardiac output physiologically by adjusting the motor speed in response to preload. A pressure or other sensor will provide the feedback signal to the electronic output control system. Figure 2 shows a block diagram of the system.

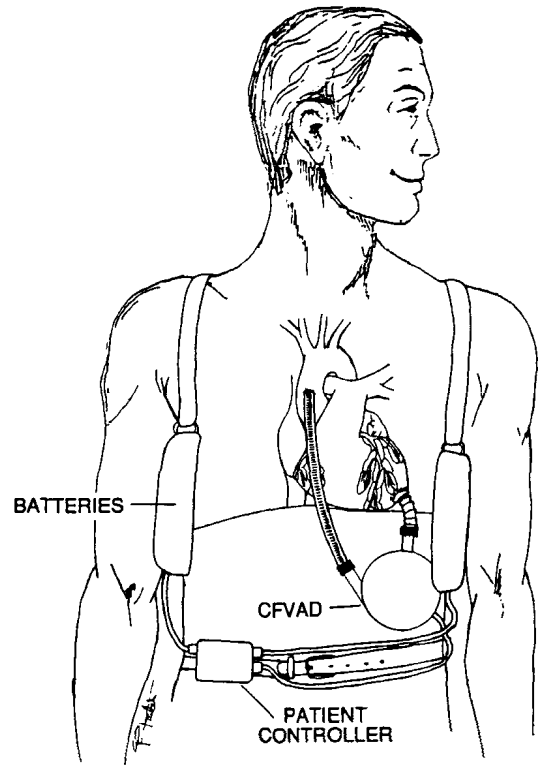

FIG. 1. This front view shows the ventricular assist pump system as it would be used in an adult.

PROTOTYPE CFVAD

The CFVAD2 consists of 5 subsystems: pump, magnetic bearings, motor, electronic control, and biocompatible-contacting surfaces. This prototype model was intended to demonstrate the concept of a small pump fully suspended in a 5-axis electromagnetic bearing system. The overall dimensions of the CFVAD2 were 175 mm (6.9 inches) in axial length and 117 mm (4.6 inches) in outer diameter. The rotor had an axial length of 105 mm (4.12 inches) and weighed 365.5 gram force (gf) (1.57 pound force [lbf]). The larger diameter impeller section had an axial length of 36 mm (1.42 inches).

A detailed drawing of the prototype is shown in Fig. 3. Fluid flows along the axial inlet of the centrifugal impeller and then outward radially into a

Abbott v. Miracor, IPR2025-00113
Abbott Ex. 1028, p. 2 of 9

15251594, 1996, 5, Downloaded from https://onlinelibrary.wiley.com/doi/10.1111/j.1525-1594.1996.tb04486.x by Mart Wagner , Wiley Online Library on [21/10/2024]. See the Terms and Conditions (https://onlinelibrary.wiley.com/terms-and-conditions) on Wiley Online Library for rules of use; OA articles are governed by the applicable Creative Commons License

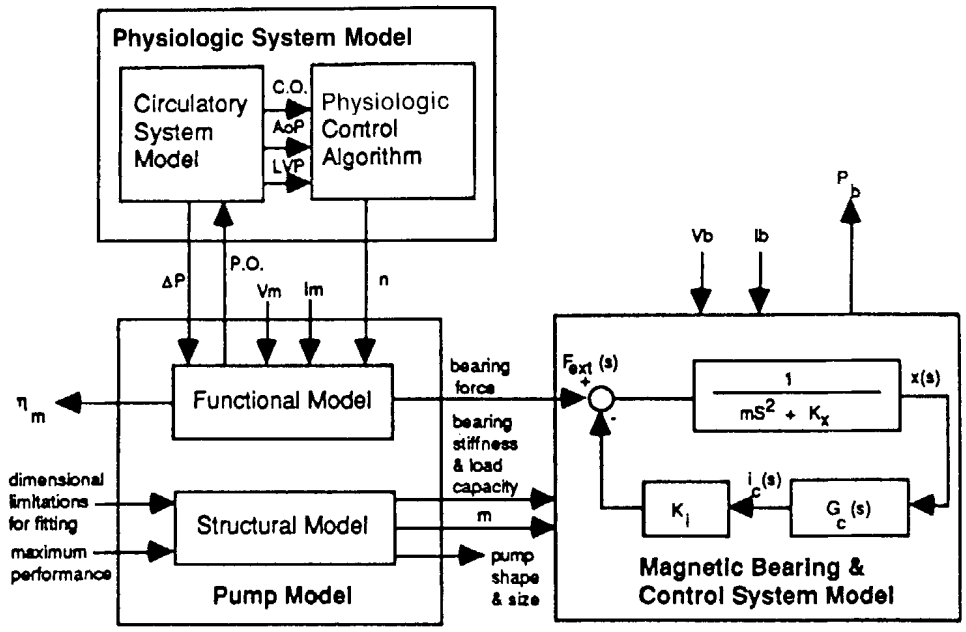

FIG. 2. The CFVAD system is depicted as a functional diagram. C.O., cardiac output; AoP, aortic pressure; LVP, left ventricular pressure; ΔP, differential pressure across pump; P.O., pump output pressure; n, motor speed; V_m, I_m, and η_m, motor voltage, current, and efficiency; m, motor mass; V_b, I_b, and P_b, magnetic bearing voltage, current, and power consumption; $G_c(s)$, controller transfer function; K_i, actuator gain; K_x, open loop stiffness; $i_c(s)$, control current; x(s), rotor position; $F_{ext}(s)$, external force.

vaneless diffuser. The motor and magnetic bearings are integrated with the pump impeller and housing as shown. The motor stator and inlet radial magnetic bearing stator are located along the inlet section. The outlet radial magnetic bearing stator and thrust bearing stator are located behind the impeller. The motor rotor, inlet radial magnetic bearing rotor, outlet radial magnetic bearing rotor, and magnetic thrust bearing rotor all are located on the rigid rotor of the pump.

THRUST BEARINGS

Magnetic bearings, when operated essentially single sidedly, as in the case of this VAD, are non-

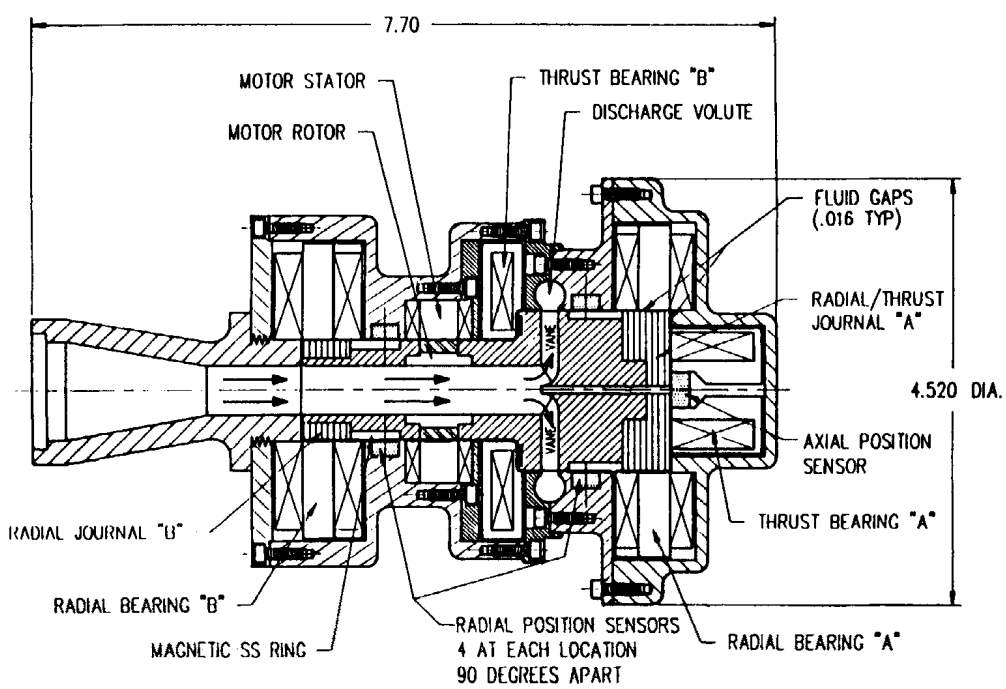

FIG. 3. This drawing shows the structure of the CFVAD2 in detail (scale: inches).

RIGHTSLINK

Abbott v. Miracor, IPR2025-00113
Abbott Ex. 1028, p. 3 of 9

15251594, 1996, 5, Downloaded from https://onlinelibrary.wiley.com/doi/10.1111/j.1525-1594.1996.tb04486.x by Matt Wagner , Wiley Online Library on [21/10/2024]. See the Terms and Conditions (https://onlinelibrary.wiley.com/terms-and-conditions) on Wiley Online Library for rules of use; OA articles are governed by the applicable Creative Commons License

linear. The force is related to the square of the coil currents, as described by Allaire et al. (11,17,18). The force F, which attracts the rotor in a single-sided stator, is given by

$$F = \frac{B^2 A_g}{\mu_0} = \epsilon \frac{\mu_0 N^2 I^2 A_g}{4G^2} \quad (1)$$

The term ϵ represents the correction for leakage and fringing, and it has a value of approximately 0.9 for thrust bearings.

Then, F can be expressed as

$$F = K_{Ti} I^2 \quad (2)$$

where the nonlinear current gain constant K_{Ti} is given by

$$K_{Ti} = \epsilon \frac{\mu_0 A_g N^2}{4G_0^2} \quad (3)$$

for a single-sided thrust bearing. For a given bearing configuration, all of these parameters are known. It may be noted that this equation differs from the normal practice in magnetic bearings, which models the force as a linear actuator gain and a linear open loop stiffness term (11), as indicated in Fig. 2. The open loop stiffness term is assumed to be small in the following and is neglected.

The thrust bearing was divided into 2 parts: thrust bearing A located at the back of the impeller and thrust bearing B located in front of the impeller. The geometry for thrust bearing A is shown in Fig. 4. The outer pole geometry has an outer diameter (OD) of 33.0 mm (1.30 inches), an ID of 28.44 mm (1.12 inches), and a length (L) of 22.9 mm (0.90 inches). The bearing magnetic material was silicon iron with a saturation flux density of approximately 1.3 Tesla (T). The thrust collar was constructed of material larger in diameter than the outer pole geometry, but the effective geometry is the same as the dimensions given above. The details of thrust bearing B are not given in this article. The design RMS thrust force for thrust A was 908 gf (2.0 lbf) and for thrust B was 1,820 gf (4 lbf).

The magnetic bearings support the pump rotor and prevent it from contacting or coming close to the stationary housing. An active control system is used for the thrust bearings with an analog proportional-derivative-integral (PID) control system (15). The position feedback control signal was provided by an eddy current sensor, as illustrated in Fig. 2.

Magnetic bearings tend to have large clearances, in the range of 0.3 to 1.0 mm (0.010 to 0.040 inches), which is very good for high flow rates in the clearances and for low shear. However, it should be noted that the active control system keeps the actual shaft motions in the range of 0.03 to 0.05 mm (0.001 to 0.002 inches) in amplitude.

Measurements were conducted on the rotor to evaluate the bearing current gain constant. For the double-acting bearing configuration, the governing equation is

$$F = M_r g = [K_{T1} I_{T1}^2 - K_{T2} I_{T2}^2] \quad (4)$$

The bearing was placed in the configuration where the gravitational load was along the axis of the pump, as illustrated in Fig. 5. The rotor mass weight was 365 gf (0.804 lbf). Four cases were considered (Table 1). The first two cases yield the results

$$K_{T1} = 1.00 \text{ kg-f/A}^2 \text{ and } K_{T2} = 0.721 \text{ kg-f/A}^2 \quad (5)$$

whereas the second set of cases yields

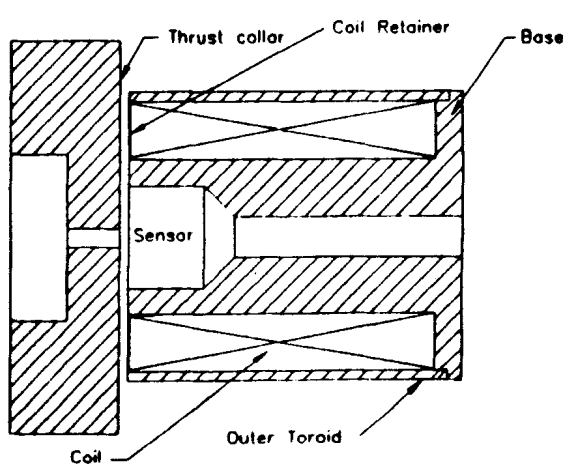

FIG. 4. The geometry of thrust bearing A (located behind impeller) is shown.

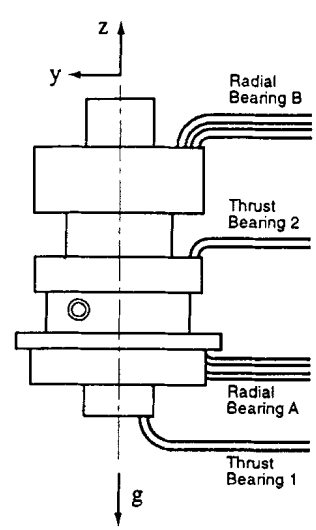

FIG. 5. The orientation is shown for the thrust bearing tests.

Abbott v. Miracor, IPR2025-00113
Abbott Ex. 1028, p. 4 of 9

15251594, 1996, 5, Downloaded from https://onlinelibrary.wiley.com/doi/10.1111/j.1525-1594.1996.tb04486.x by Matt Wagner , Wiley Online Library on [21/10/2024]. See the Terms and Conditions (https://onlinelibrary.wiley.com/terms-and-conditions) on Wiley Online Library for rules of use; OA articles are governed by the applicable Creative Commons License

TABLE 1. *Measured thrust bearing currents*

Bias current	Loading conditions	I_{T1} (mA)	I_{T2} (mA)
No bias	z parallel to g	597	0
No bias	−z parallel to g	0	712
Bias	z parallel to g	785	596
Bias	−z parallel to g	440	910

$$K_{T1} = 0.979 \text{ kg-f/A}^2 \text{ and } K_{T2} = 0.670 \text{ kg-f/A}^2 \quad (6)$$

These results are reasonably close in value. The average value was employed for further calculations.

RADIAL BEARINGS

The radial bearing (A) at the outlet side has a 16-pole, planar, radial bearing stator (Fig. 6). It has an OD of 89.5 mm (3.52 inches), an ID of 43.4 mm (1.71 inches), and a length of 8.2 mm (0.0322 inches). The journal had an OD of 42.4 mm (1.67 inches), an ID of 3.30 mm (1.30 inches), and a radial clearance of 0.406 mm (0.016 inches). The design RMS load capacity was 2,270 gf (5 lbf) as calculated by the methods presented in Allaire et al. (11).

The inlet side radial bearing (B) stator (not shown in Fig. 6) is placed at the OD of the impeller. It has an OD of 79.4 mm (3.12 inches), an ID of 26.9 mm (1.06 inches), and a length of 0.406 mm (0.322 inches). The rotor has an OD of 25.4 mm (1.00 inches), an ID of 15.6 mm (0.611 inches), and a clearance of 0.406 mm (0.016 inches). The design RMS load capacity is 907 gf (4 lbf). The control system was analog PID, and the sensors were eddy current sensors with the locations indicated in Fig. 3.

The rotor was placed in the horizontal orientation (with the Z axis perpendicular to gravity). The force balance in the Y direction is

$$f_A + f_B = M_r g \quad (7)$$

Let the angle θ represent the angular position of the rotor in the X-Y plane. Figure 7 shows the orientations. Here, for bearing A, θ_A is the angle of the magnetic gap, where $\theta_A = 0$ for S4B at +X and S2B at +Y. Similarly θ_B represents the angle of magnetic gaps for bearing B where $\theta_B = 0$ corresponds to the magnetic gap S4B is at +X and S3B is at +Y. Both θ_A and θ_B have positive values in the counterclockwise direction. The two bearing are oriented so that the angle between the magnetic gaps is $\theta_B - \theta_A = 20$ degrees between the bearings.

Applying the force balance condition to all of the magnetic gaps yields the equation

$$K_{1A}I_{1A}^2\sin\theta_A - K_{1B}I_{1B}^2\sin\theta_A - K_{2A}I_{2A}^2\cos\theta_A + K_{2B}I_{2B}^2\cos\theta_A - K_{3A}I_{3A}^2\cos\theta_B + K_{3B}I_{3B}^2\cos\theta_B - K_{4A}I_{4A}^2\sin\theta_B + K_{4B}I_{4B}^2\sin\theta_B = M_r g \quad (8)$$

This equation is employed for each n measurement. In general, this set of n equations can be written as

$$[F_F][K] = [M_r g] \quad (9)$$

where $[F_F]$ is n × 1, $[K]$ is 8 × 1, and $[M_r g]$ is n × 1.

The moment balance equation is

$$kf_A - (1 - k)f_B = 0 \quad (10)$$

and k is the distance between the A bearing force and the center of gravity. For this rotor, $k = 0.3$. The moment balance is applied in the same manner as the force balance with the result

$$k[K_{1A}I_{1A}^2\sin\theta_A - K_{1B}I_{1B}^2\sin\theta_A - K_{2A}I_{2A}^2\cos\theta_A + K_{2B}I_{2B}^2\cos\theta_A] - (1 - k)[-K_{3A}I_{3A}^2\cos\theta_B - K_{3B}I_{3B}^2\cos\theta_B - K_{4A}I_{4A}^2\sin\theta_B + K_{4B}I_{4B}^2\sin\theta_B] = 0 \quad (11)$$

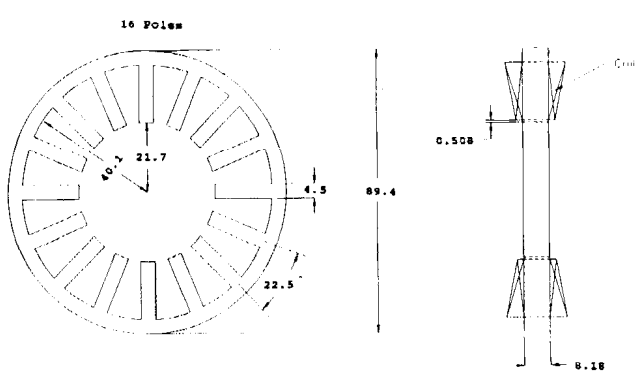

FIG. 6. The geometry of radial bearing A (located Behind the Impeller) is shown.

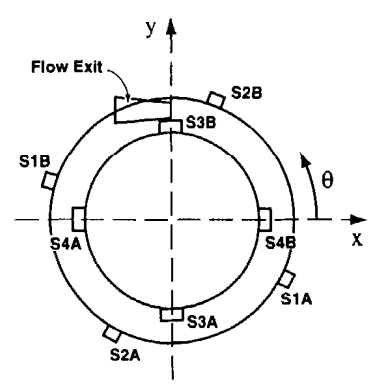

FIG. 7. The angular positions of the radial bearings are shown.

RIGHTSLINK

Abbott v. Miracor, IPR2025-00113
Abbott Ex. 1028, p. 5 of 9

15251594, 1996, 5, Downloaded from https://onlinelibrary.wiley.com/doi/10.1111/j.1525-1594.1996.tb04486.x by Matt Wagner , Wiley Online Library on [21/10/2024]. See the Terms and Conditions (https://onlinelibrary.wiley.com/terms-and-conditions) on Wiley Online Library for rules of use; OA articles are governed by the applicable Creative Commons License

Again, this equation is applied to each n measurement. In general, this set of n equations is written as

$$[F_M][K] = [0] \tag{12}$$

where $[F_M]$ is n × 1, $[K]$ is 8 × 1, and the right-hand side is n × 1.

Measurements of currents were made with θ_B = 0, 45, 90, −45, −90, and −135 degrees, and $\theta_A = \theta_B - 20$. Also, measurements of current were made with θ_A = 0, 45, −45, −90, −135, −180 degrees and $\theta_B = \theta_A + 20$ degrees. The data are not presented.

The set of simultaneous equations for the nonlinear current gains has the general form

$$[F][K] = [M] \tag{13}$$

where

$$[F] = \begin{bmatrix} [F_F] \\ [F_M] \end{bmatrix} \text{ and } [M] = \begin{bmatrix} [M_r g] \\ [0] \end{bmatrix} \tag{14}$$

The least squares estimation of the $[K]$ matrix is given by

$$[\hat{K}] = ([F]^T[F])^{-1}[F]^T[M] \tag{15}$$

The final results are

$$[\hat{K}] = \begin{bmatrix} K_{1A} \\ K_{1B} \\ K_{2A} \\ K_{2B} \\ K_{3A} \\ K_{3B} \\ K_{4A} \\ K_{4B} \end{bmatrix} = \begin{bmatrix} 0.653 \\ 0.522 \\ 0.581 \\ 0.550 \\ 0.378 \\ 0.795 \\ 0.486 \\ 0.715 \end{bmatrix} (\text{kgf/A}^2) \tag{16}$$

These values are employed in the determination of the bearing forces for which the coefficient matrix is 2n × 8, the $[K]$ matrix is 8 × 1, and the right-hand side is 2n × 1.

FORCES ACTING ON THE ROTOR

In this first fully electromagnetic bearing supported prototype, a number of external forces acting on the impeller were unknown. These included fluid forces (19), unbalance forces, motor eccentricity magnetic forces, and others. Thus, the magnetic bearings were significantly overdesigned compared to the actual measured forces. One of the primary purposes for the development of CFVAD2 was the ability to measure the imposed forces on the pump rotor.

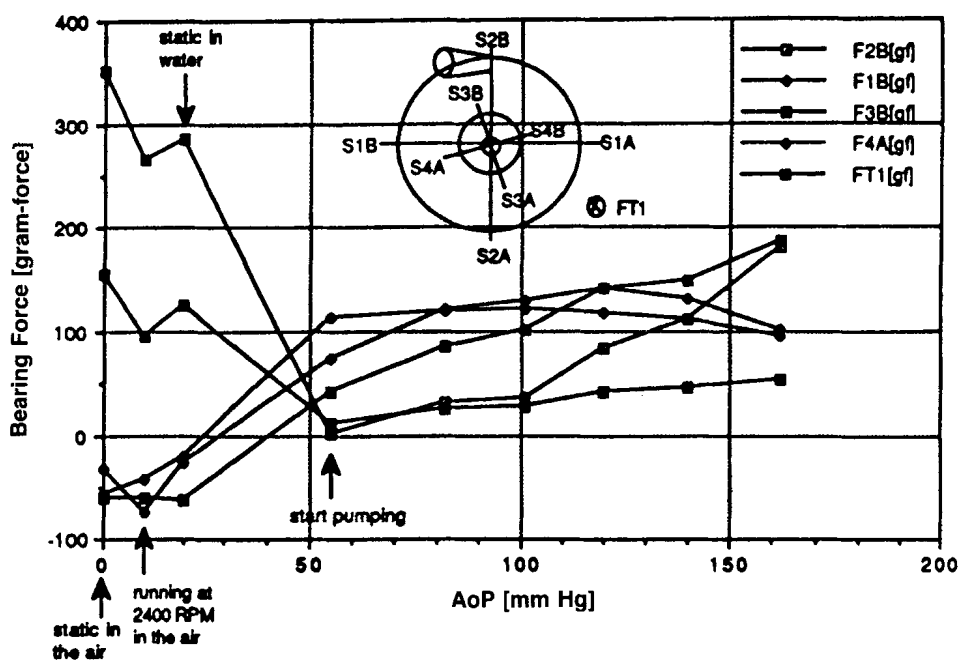

FIG. 8. The experimentally measured forces exerted by the magnetic bearings are shown.

Abbott v. Miracor, IPR2025-00113
Abbott Ex. 1028, p. 6 of 9

15251594, 1996, 5, Downloaded from https://onlinelibrary.wiley.com/doi/10.1111/j.1525-1594.1996.tb04486.x by Matt Wagner , Wiley Online Library on [21/10/2024]. See the Terms and Conditions (https://onlinelibrary.wiley.com/terms-and-conditions) on Wiley Online Library for rules of use; OA articles are governed by the applicable Creative Commons License

The bearing coil currents were measured, and 10 forces, that is, 8 radial and 2 axial that act on the rotor, were calculated based on the actuator current gains given in Eqs. 5 and 6 (16). The radial forces plotted were the forces F1B and F2B, at the impeller end of the rotor; F3B and F4A, at the inlet end of the rotor, were plotted in Fig. 8 relative to the aortic pressure (AoP), which ranged from 55 mm Hg to 160 mm Hg.

The initial static forces in air, with the rotor oriented horizontally, are shown in the first set of data points. It may be noted that the measured static vertical force, F2B = 350 gf (1.54 lbf) is relatively near the center of gravity whereas the weight of the rotor is 365 gf (1.61 lbf). At the impeller end, the radial force was 150 gf (0.66 lbf), and the other forces were small. The next set of data points shown is the rotor running at 2,400 rpm in air, and the radial forces are shown to drop somewhat because of the rotation effects.

Results with the impeller in water are shown in Fig. 8. The measured static forces in water are similar to the static forces in air. As the pump rotor started rotating and pumping, the forces were measured. All of the forces dropped to approximately 150 gf (0.66 lbf) for all measured forces up to a pressure of 150 mm Hg apparently because of fluid clearance effects in the water that help to center the impeller. Axial flow seals in industrial pumps are well known to produce similar centering forces and positive stiffness effects (20).

The measured total power delivered to the prototype magnetic bearings was approximately 50 W (10 V and approximately 5 A). Most of this power was dissipated in the resistance losses because of bias currents of approximately 0.7 amps to each of the magnetic bearing coils.

PUMP PERFORMANCE TESTING

The pump was tested for pressure increase and efficiency with the CFVAD2 unit connected to a simple mock circulation system (in a benchtop test) pumping water. The water was circulated with a physiologic level of pump output and differential pressure. Pump inlet pressure (left arterial pressure) and pump outlet pressure (aortic pressure) and volume flow rate were measured. Figure 9 shows the measured differential pressure head versus the flow rate at various rotor rotation rates. A typical flow of 6 L/min was achieved against a differential pressure of 100 mm Hg at 38 Hz (2,300 rpm). A range of pressure heads versus flow rate characteristics may be obtained from this pump with small variations in the pump rotation speed.

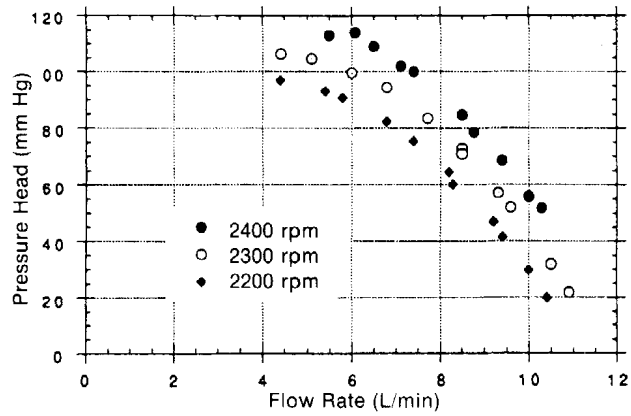

FIG. 9. The measured pressure is graphed relative to the flow for various rotational speeds with the CFVAD attached to mock circulation system in a benchtop test.

Figure 10 shows the efficiency curves versus the flow rate at the same rotation rates. The pump impeller was designed to have peak efficiency at approximately 6 L/min (in the normal physiological range for humans), and the measured pump efficiency has a peak of approximately 55% at that flow rate. The curve shows the expected drop off in efficiency at higher flow rates. It is clear that the CFVAD2 meets the necessary flow requirements for a ventricular assist device.

IN VITRO BLOOD PUMPING TESTS

The CFVAD performance was studied while pumping blood in vitro. Fresh bovine blood (1.5 L) was collected and anticoagulated following a standard method developed by Garrison et al. (21). The blood was pumped at a constant rate (5 L/min) at

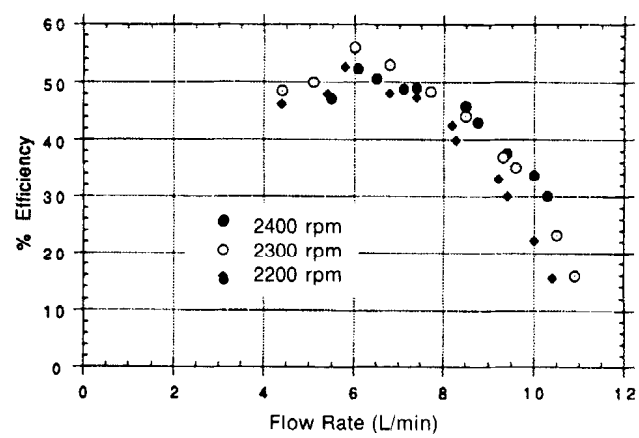

FIG. 10. The measured pump efficiency is plotted relative to the flow for various rotational speeds with the CFVAD attached to a mock circulation system in a benchtop test.

Abbott v. Miracor, IPR2025-00113
Abbott Ex. 1028, p. 7 of 9

15251594, 1996, 5, Downloaded from https://onlinelibrary.wiley.com/doi/10.1111/j.1525-1594.1996.tb04486.x by Matt Wagner , Wiley Online Library on [21/10/2024]. See the Terms and Conditions (https://onlinelibrary.wiley.com/terms-and-conditions) on Wiley Online Library for rules of use; OA articles are governed by the applicable Creative Commons License

room temperature for 4 h. Blood samples were taken every half hour and were centrifuged at 1,500 g for 15 min. The supernate was removed carefully for quantification of plasma-free hemoglobin using a Beckman DU-7 spectrophotometer. Three separate experiments were conducted with the CFVAD2 system. The results of a typical experiment are shown in Fig. 11. The averages of the 3 experiments are similar to the results shown in Fig. 11.

The results show that during the 4 h recirculation the overall average cumulative, plasma-free hemoglobin level increased by less than a factor of 2 from the baseline value (the maximum was 1.9 times the baseline value). This result is very encouraging considering that the product of the product of hemolysis (PfHb) represents a cumulative value where all of the products of hemolysis remain in the blood throughout the experiment. During in vivo experiments, hemoglobin released in the blood is continuously removed biologically. The average overall index of hemolysis for the 3 experiments, was 0.0086 ± 0.0012 where the index of hemolysis (IH) is defined by Koller and Hawrylenko (22):

$$IH = \frac{V(100 - HK)\Delta fHb}{100\ TF} \tag{17}$$

where V is the blood filling volume (L), HK is the hematocrit (%), ΔfHb is the increase in plasma-free hemoglobin (mg/dl), F is the flow rate (L/min), and T is the total pumping time (min). This hemolysis level is comparable to that achieved by the St. Jude Isoflow pump (0.0082 ± 0.0009) at 6 L/min under similar test conditions as reported by Mulder et al. (23).

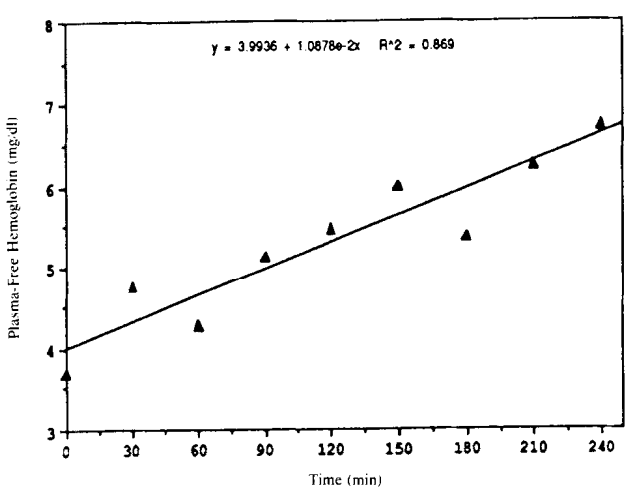

FIG. 11. The value of plasma-free hemoglobin is graphed relative to time produced in the CFVAD2.

CONCLUSIONS

A prototype, continuous flow, electromagnetic bearing supported ventricular assist device has been levitated and rotated successfully. The magnetic bearings operated successfully, centering the rotor in the clearance passages. A method was developed to measure the nonlinear gain constants for each of 10 magnetic gaps in the pump by measuring bearing coil currents in various orientations with respect to gravitational loading. These gain constants were then employed to evaluate the external forces acting on the impeller. It was found that the radial forces on the impeller were significantly lower than expected, probably because of the stiffness and damping effects of the fluid in the clearance passages.

The hemolysis rates demonstrate that the CFVAD2 pump circulates blood without significant damage to the blood cells. The observations illustrated in this article show that the rate of hemoglobin release was approximately 0.65 mg/dl/h, a very encouraging result. The current impeller design has achieved hemolysis levels comparable to those achieved by other clinically used and accepted centrifugal blood pumps.

The current prototype has several disadvantages. It is at least twice the desirable size for implantation, and the weight is too high. The power loss is too high, and too many wires are employed. However, although it has some shortcomings, the CFVAD2 prototype is apparently the first fully electromagnetically supported ventricular assist device. It has been quite successful as a test apparatus. Work is proceeding on the next version of this magnetic bearing supported continuous flow ventricular assist device (CFVAD3) to reduce the size, weight, power loss, and wire count. A pancake impeller with much smaller magnetic bearings (appropriate for the measured forces) and self-sensing (eliminating the space and wires for sensors) is being designed now.

NOMENCLATURE

A_g area of airgap
B magnetic flux density
f radial force
F axial force
g gravitational constant in y direction
G airgap length
I coil current
k distance to radial bearing A
K_T current gain constant
M_r mass of rotor

Abbott v. Miracor, IPR2025-00113
Abbott Ex. 1028, p. 8 of 9

15251594, 1996, 5, Downloaded from https://onlinelibrary.wiley.com/doi/10.1111/j.1525-1594.1996.tb04486.x by Matt Wagner , Wiley Online Library on [21/10/2024]. See the Terms and Conditions (https://onlinelibrary.wiley.com/terms-and-conditions) on Wiley Online Library for rules of use; OA articles are governed by the applicable Creative Commons License

N number of coil turns
R reluctance
x horizontal coordinate
y vertical coordinate
z axial coordinate
μ_0 permeability of free space
θ orientation angle of rotor
ϵ force derating factor

REFERENCES

1. Joyce LD, Kiser JC, Eales F, King RM. Experience with the Sarns centrifugal pump as a ventricular assist device. *Trans Am Soc Artif Intern Organs* 1990;36:M619–22.
2. Noon GP. Bio-Medicus ventricular assistance. *Ann Thorac Surg* 1991;52:180–1.
3. Olsen DB, Wampler RK. Continuous blood-flow pumps with internal and external motors. *Proceedings of the International Workshop on Rotary Blood Pumps*, Vienna, Austria, 1988:8–17.
4. Wampler RK, Moise JC, Frasier OW, Olsen DB. In vivo evaluation of a peripheral vascular access axial flow blood pump. *Trans Am Soc Artif Inter Organs* 1988;34(3):450–4.
5. Macris MP, Myers TJ, Jarvik R, Robinson JL, Fuqua JM, Parnis SM, Frazier OH. In vivo evaluation of an intraventricular electrical axial flow pump. In: Attar S, ed. *New developments in the cardiac assist devices*. New York: Praeger, 1984:54–78.
6. Butler K, Maher T, Borovetz H,Litwak P, Kormos R. (abstract 16) Second Congress of the International Society of Rotary Blood Pumps, 1994, Tokyo, Japan.
7. Akamatsu T, Shiroyama T, Fukumasu H. Development of nutating centrifugal blood pump. *Proceedings of the 2nd International Symposium on Artificial Heart and Assist Devices, Tokyo*. 1989:107–12.
8. Akamatsu T, Nakazeki T, Itoh H. Centrifugal blood pump with a magnetically suspended impeller. *Artif Organs* 1992:305–7.
9. Akamatsu T, Yoshino Y, Tsukiya T, et al. Studies of performance and operating condition of the centrifugal blood pump with magnetically suspended impeller (abstract). *Artif Organs* 1994;18:244.
10. O'Hara Y, Nosé Y. The next generation Baylor C-Gyro pump: antithrombogenic free impeller design for long term centrifugal VAD. *Artif Organs* 1994;18:238–43.
11. Allaire PE, Maslen EH, Humphris RR, Knospe CR, Lewis DW. Magnetic bearings. In: *Handbook of Lubrication and Tribology*. CRC Press, 1994;III:577–600, Boca Raton, FL.
12. Bramm G, Novak P, Olsen DB. Blood pump for long term application with magnetically suspended rotor to reduce blood trauma. 2nd International Workshop of The Austrian Society of Artificial Organs, 1981;II:26–9, Vienna, Austria.
13. Olsen DB, Bramm G. Blood pump with magnetically suspended impeller. *Trans Am Soc Artif Intern Organs* 1985;31:395–401.
14. Allaire P, Imlach J, McDonald J, Humphris R, Lewis D, Blair B, Claydon J, Flack R. Design, construction, and test of a magnetic bearing in an industrial canned motor pump. Proceedings of Texas A&M Pump Symposium, Houston, Texas, May 1989.
15. Allaire PE, Maslen EH, Lewis DW, Flack RD. Magnetic thrust bearing operation and industrial pump application. Presented at the American Society of Mechanical Engineering Turbo Expo '94: Land, Sea and Air Conference, The Hague, June 13–16, 1994.
16. Allaire PE, Marlen EH, Kim HC, Olsen DB, Bearnson GD. *Prototype Ventricular Assist Device Supported on Magnetic Bearings*, Proceedings of MAG 95, Technomics, Lancaster, PA; 63–76.
17. Allaire PE. Design and test of a magnetic thrust bearing. *Journal of the Franklin Institute* 1989;326(6).
18. Allaire PE, Fittro RL, Maslen EH, Wakefield WC. Current/force relations in solid magnetic thrust bearings. Proceedings of REVOLVE '94, Calgary, Alberta, Canada, June 7–, 1994.
19. Flack RD, Allaire PE. Lateral forces on pump impellers: a literature review. *Shock and Vibration Digest* 1984;16(1): 5–14.
20. Allaire PE, Lee CC, Gunter EJ. Dynamics of short eccentric plain seals with high axial Reynolds number. *Journal of Spacecraft and Rockets* 1978;15(6):341–7.
21. Garrison LA, Frangos JA, Geselowitz DB, et al. A new mock circulatory loop and its application to the study of chemical additive and aortic pressure effects on hemolysis in the Penn State ventricular assist device. *Artif Organs* 1994;18:397–407.
22. Koller T, Hawrylenko A. Contribution to the in vitro testing of pump extracorporeal circulation. *J Cardiovasc Surg* 1967;54:22–9.
23. Mulder MM, Hansen AC, Mohammad SF, Olsen DB. In vitro investigation of the St. Jude Medical Isoflow centrifugal pump: flow visualization and hemolysis studies. *Artif Organs* (in press).

RIGHTSLINK

Abbott v. Miracor, IPR2025-00113
Abbott Ex. 1028, p. 9 of 9

15251594, 1996, 5, Downloaded from https://onlinelibrary.wiley.com/doi/10.1111/j.1525-1594.1996.tb04486.x by Matt Wagner , Wiley Online Library on [21/10/2024]. See the Terms and Conditions (https://onlinelibrary.wiley.com/terms-and-conditions) on Wiley Online Library for rules of use; OA articles are governed by the applicable Creative Commons License